Lawrence Berkeley National Laboratory

Title
HIGH RESOLUTION TECHNIQUES AND APPLICATION TO NON-OXIDE CERAMICS

Permalink
https://escholarship.org/uc/item/14n070k7

Author
Clarke, D.R.

Publication Date
1977-10-01

UC-25
UC-37

HIGH RESOLUTION TECHNIQUES AND
APPLICATION TO NON-OXIDE CERAMICS

David R. Clarke

October 1977

HIGH RESOLUTION TECHNIQUES AND APPLICATION TO NON-OXIDE CERAMICS

David R. Clarke

Department of Materials Science and Mineral Engineering
University of California, Berkeley, California 94720.

ABSTRACT

The microstructure of ceramic materials can now be observed directly at the atomic level by using high resolution electron microscopy. These techniques are described in detail and the type of new information that they are revealing about the structure of ceramics is illustrated with examples drawn from investigations of hot-pressed silicon nitrides, sintered silicon carbide and a "Sialon" system.

I. INTRODUCTION

It is now practicable to examine the microstructure of ceramics directly at the atomic level. This exciting development has become possible with the use of high resolution electron microscopy coupled with the ability to prepare suitable specimens for such work. Already a wealth of new information about the structure of ceramics has been revealed. The purpose of this paper is two-fold: firstly, to describe the techniques of high resolution electron microscopy (including both the fundamental principles and the practical steps involved); and secondly, to illustrate the impact of high resolution electron microscopy on the study of ceramics with examples from a series of investigations into non-oxide systems. The particular examples presented are drawn from investigations into (i) the detection of intergranular phases in hot pressed silicon nitride, (ii) the mechanism of the phase transformation in silicon carbide and (iii) the crystal structure refinement of a phase in the prototype "Sialon" Si-Al-O-N system.

II. HIGH RESOLUTION ELECTRON MICROSCOPY TECHNIQUES

The term high resolution electron microscopy has been applied to a wide variety of microscopy techniques such as weak beam dark-field imaging[1], high order bright field imaging[2] and strioscopic imaging[3], but here it is restricted to methods that provide images in which either the crystal lattice planes or the projection of the individual atoms in the crystal are recorded. The former has come to be known as lattice fringe imaging and the latter as structure imaging.

Although the technique of lattice fringe imaging was first demon-strated in 1956, when Menter observed the 12Å spacing (20$\bar{1}$) lattice planes

in platinum phthalocyanine[4], its application to materials science in general and to ceramics in particular has had to await the development of microscopes having a line resolution of about 2Å. Also, in common with other attempts to apply electron microscopy to ceramics, it had to await the introduction of specimen preparation by ion beam thinning pioneered in this country by Tighe[5]. Now it has reached the point where any skilled microscopist, with access to a high resolution microscope, can apply the technique. For this reason, the fundamental factors affecting contrast in the lattice image, the optimum experimental conditions and the practical steps taken to obtain the lattice image are described in the following sections.

(1) Fundamentals

In this section the fundamental factors that determine both the formation and contrast of lattice images will be discussed on the basis of the optical principles involved.

The formation of both lattice fringe images and lattice structure images can be understood in terms of the Abbe diffraction theory of imaging[6]. Although this was originally developed to describe image formation in the optical microscope it is equally applicable to imaging in the electron microscope. Its details[7] are beyond the scope of this presentation and therefore a simplification based on geometric optics is discussed here.

Fig. 1 is a schematic ray diagram often used to describe image formation in the optical microscope, which can also equally be used to describe the formation of a lattice fringe image in the transmission electron microscope. A parallel beam of electrons is incident on a thin foil specimen which is located just above the objective lens. The crystal lattice

planes in the foil diffract the incident illumination, according to Bragg's law, into a number of orders or beams (five in Fig. 1). The action of the objective lens is to focus these to points at the back focal plane where a moveable aperture is positioned. Some of the diffracted beams (two in this case) are allowed to pass through the aperture so that they can optically interfere to form a fringe pattern on a screen or photographic plate located at the image plane. The fringe pattern formed has the same periodicity as the spacing of the diffracting planes in the crystal, but enlarged by the imaging lenses of the microscope.

This mode of microscopy, in which the image is formed by the recombination of a number of diffracted beams is known as "phase contrast microscopy" since the contrast is influenced by the _relative_ phases of the diffracted beams interfering with one another. Despite its simplicity this model represents approximately the essential features of lattice imaging, provided that the specimen is thin enough that the electron beam undergoes only kinematical scattering in the sample.

Two types of phase change occur. The first is that which would be introduced by a perfect lens and is merely due to differences in geometric path length. The second type is introduced by the aberrations of the lens and results in an alteration of the path lengths. Since these effects are additive, they can be discussed separately.

The geometric phase difference is controlled, as seen from Fig. 1 by the angle of the diffracted beam to the optic axis of the microscope. This may be altered by either changing the spacing of the lattice planes or by tilting the incident illumination. For instance, in the schematic diagram the two beams selected by the objective aperture, the transmitted

beam, 0, and the first diffracted beam, g, both travel paths of the same length because the incident beam is tilted by β_B (Bragg angle). Thus they are exactly in phase and interfere constructively.

The effect of the spherical aberration of the objective lens is to introduce a phase delay of

$$\frac{-2\pi}{\lambda} \, c_s \theta^4$$

to a beam diffracted by an angle of θ to the optic axis[8]. The phase delay is proportional to the fourth power of the angle θ, and does not depend on the sign of the angle. Thus, for beams equally inclined to the optic axis but in opposite directions, as in Figure 1, the phase delays caused by spherical aberration cancel. This is the basis of the tilted illumination two beam method originally introduced by Dowell[9] to obtain high resolution fringe images, and remains today as the principle method used to reveal atomic detail in metals and close-packed ceramics with presently available 100 kV electron microscopes.

The relative phases may also be altered by the objective lens focus (Δf) according to the expression[8]

$$\frac{\pi}{\lambda} \, \Delta f \, \theta^2.$$

In practice, this phase change is used to compensate for the effect of spherical aberration and an optimum value of defocus can be defined at which the phase delay produced by both spherical aberration and lens defocus is minimised[10]. For conventional 100 kV electron microscopes having spherical aberration coefficients of about 1.8 mm the optimum defocus when performing many-beam structure imaging with axial illumination is approximately 900Å[7].

Consideration of the Abbe theory and of the simple geometric ray diagram enables a statement to be made about the information contained in the image. According to the theory, if the potential field created by the atomic distribution in the specimen is expressed as a Fourier expansion, the amplitude of a diffracted beam, g, is related to the gth Fourier component of the potential distribution. Ideally then, by recombining together all of the diffracted beams an image with complete fidelity will be formed. However, in practice as only a limited number of beams, determined by the positioning and angular size of the objective aperture, are used to create the image, it will only contain the spatial information having the spatial frequencies associated with these beams. For instance, in the case schematically illustrated in Fig. 1, the only spatial information conveyed corresponds to the largest crystal spacing. The information limitation is vividly illustrated by the calcultions of O'Keefe of structure images of niobium oxides[11]. As the number of diffracted beams included in the image is increased so the image more closely resembles the atomic structure.

The tilted illumination two beam imaging mode illustrated in Fig. 1 is just one of a number of possible modes that can be used to obtain lattice images. The three most common are compared in Fig. 2 in which the geometry of the diffraction pattern and the objective aperture in the back focal plane of the objective lens are schematically illustrated. In the two beam tilted illumination case, Fig. 2a, the optic axis of the microscope is situated midway between the transmitted and diffracted beam and is also the center of the objective aperture. Structure images are normally formed using the imaging configuration of Fig. 2b, in which axial illumination is used, the objective aperture is centered on the optic axis,

and the crystal oriented with a zone axis coincident with the optic axis. An alternative many-beam arrangement, known as dark-field structure imaging, is shown in Fig. 2c. In this case the illumination is no longer axial, but tilted so that the transmitted beam is off the optic axis.

(2) Optimum Experimental Conditions

The electron-optical factors established in the previous section only determine whether an image will in principle be formed and so represent the necessary conditions. In practice, however, a number of additional experimental factors affect whether the image actually formed best represents the structure of the specimen[12]. These include the specimen thickness, the specimen orientation, the accelerating voltage, the objective aperture size and the objective lens defocus. The optimum experimental conditions can only be determined by calculation of the lattice images based upon the dynamical theory of electron diffraction[7,12]. Nevertheless, a number of guidelines have been established from these calculations that are useful in determining the approximate conditions[12,13].

Firstly, the specimen must be very thin. For instance, at 100 kV a structure image with a resolution of $\leq 5\text{Å}$ can be directly interpreted in terms of the projected charge density of the object only when the sample is no thicker than about 50Å[14]. The condition for an interpretable lattice fringe image is less stringent since in general there are fewer spatial frequencies contributing to the image. However, it is still necessary to have a specimen thickness of less than about half the minimum extinction distance of all the contributing diffracted beams, typically less that approximately 600Å. Additionally, a very thin specimen is desirable so that sufficient electron intensity is transmitted for

observations to be made at high magnifications. The production of such thin ceramic specimens is a problem, but with care they can be made by either ion-thinning of a bulk material or by crushing to form thin fracture fragments.

Secondly, the specimens must be carefully oriented so that the structural features that are of interest lie exactly parallel to the direction of the incident electron beam. In the case of structural imaging the crystal should be oriented so that the electron beam is parallel to an important crystallographic direction in the crystal with crystallographically equivalent reflections in the electron diffraction pattern being of equal intensity; this requires an accuracy in alignment within a fraction of a degree[13]. For lattice fringe imaging the crystal must be oriented for a systematic set of reflections with the planes to be imaged at the exact Bragg condition.

Thirdly, the microscope must be accurately defocussed[10, 7, 12]. For structure imaging the defocus is about 800Å, which corresponds to the optimum for a weak phase object. It is found that changes in focus from this value by more than about 200Å gives rise to images which bear little apparent relationship to the actual structure[7]. In the case of two beam tilted illumination the optimum defocus occurs when there is a direct superposition of the two images ($\Delta f = 0$).

The optimum objective aperture is one that will transmit only the diffracted beams corresponding on the image resolution required, and cut off the remainder. This is necessary since additional beams will only add to the background and reduce the overall contrast of the image.

(3)   Practical Operation

In order to obtain lattice images the microscope must be operated at or close to the limit of its capabilities and for this reason particular care must be taken to ensure that the optimum experimental conditions are fulfilled and that the microscope is fully aligned.

There are basically seven steps for recording a lattice image, the first three of which are carried out in the diffraction mode of operation. (1) The specimen is tilted and/or translated until a suitable orientation is found.   (2) The electron diffraction pattern is then centered on the optic axis and the illumination adjusted for tilted-illumination two beam imaging, structure imaging, or dark field imaging (figure 2a-c respectively) as desired.   In the case of two beam tilted illumination imaging (figure 2a) the beams must be accurately positioned so that the midpoint between the transmitted beam and the strongly diffracted beam lies on the optic axis, so that the phase delays introduced by spherical aberration cancel.   (3) An objective aperture just large enough to enclose the beams of interest is inserted and carefully positioned to be centered about the optic axis.   (4) In the image mode the magnification of the area to be imaged is increased and an approximate focus setting is obtained.   Near to the exact focus position, the various specimen images which correspond to each beam transmitted by the objective aperture can be made to shift with respect to one another by small changes in the objective lens current, and at the Gaussian focal point they all superimpose.   (5) At high magnifications the image astigmatism is corrected either by using the Fresnel fringes at the edge of the specimen as a guide, or preferably by using the background

texture of the image [8]. (6) Final focussing and adjustment of astigmatism is carried out until a minimum in background phase contrast is observed. This is the condition of exact focus and is where the lattice fringes for the two beam imaging mode will be produced. In structure imaging the optimum objective lens defoucus value is measured from this setting. (7) Lastly a thorough focus series of photographs of the image is taken at small increments of objective lens current from the optimum defocus condition.

The electrical insulating property of many ceramics often imposes an additional requirement in obtaining a lattice image. If the specimen does charge up under the electron beam it is necessary to coat it with a thin layer of evaporated carbon. This layer increases the thickness of the specimen and so can make it more difficult to obtain a lattice image. Furthermore, if the layer of carbon is insufficiently conducting, changes in the incident illumination will affect the image astigmatism and focus. For this reason, the images must be recorded at the same magnification and illumination conditions used for the astigmatism correction and final focussing.

(4)   Image Interpretation

In common with other imaging modes of electron microscopy the interpretation of the image contrast is not always intuitively obvious. For instance Cowley [15] and later Hashimoto [16] et al. showed that the lattice fringes are displaced from the positions of the crystal potential maxima and that a reversal of contrast occurs for two beam images if the crystal thickness changes by half an extinction distance. Also they found that the fringe spacing varies with deviations from the exact

Bragg diffraction condition and only corresponded with the spacing of the crystal lattice planes at the exact Bragg angle.

In view of such complexities considerable effort has been expended in trying to establish the experimental conditions under which the image best represents the structure of the specimen, particularly in the case of a structure image. In order to do this requires computation of the electron wave propagation through the potential of the crystal structure from the appropriate n-beam dynamical electron diffraction equation [7,17]. Then the effects of objective lens defocus, size of objective aperture, spherical aberration and beam convergence must be calculated [10]. This complete computation is complex and although it has been carried out for relatively few crystals, notably complex transition element oxides, e.g. Nb_2O_5 [18,19] has nevertheless led to the guidelines mentioned in the previous section. However these are guidelines only and in crystal structure analysis the images must be calculated to ensure that the correct interpretation is made. The essential physics required to do this is described in depth elsewhere [7] and much of which has been published in a series of papers in Acta Crystallographica (Series A) [14,18-22].

The problems posed in image interpretation of lattice fringe images are less severe since in general only one fringe spacing is involved. Nevertheless, considering the large number of variables which can affect the image it is essential that the computation be carried out.

III. APPLICATIONS TO NON-OXIDE CERAMICS

(i) Grain Boundaries

Many important ceramics, particularly those formed by either liquid phase sintering or by a solution-reprecipitation process, consist of a

mixture of one or more crystalline phases and an additional "wetting"
phase. (The wetting phase may be crystalline or amorphous at room
temperature, but for the sake of brevity is referred to here simply as
a wetting phase.) When these ceramics are examined by optical microscopy
the wetting phase appears to have a near-zero contact angle with the other
phase(s) leading to the common assumption that it encompasses and
separates the grains of the crystalline phases. Whether or not it
does indeed wet the grains to form a continuous grain boundary film is of
importance in relating macroscopic properties to the observed micro-
structure of a number of materials of contemporary interest, for instance
hot pressed silicon nitride and the zinc oxide based varistor materials.
Before discussing the investigation of the grain boundaries in silicon
nitride, the extension of the technique of lattice fringe imaging to the
study of boundaries is described since it is pertinent to the general
problems of detecting grain boundaries phases and of studying the
structure of the grain boundary itself.

a) Technique

Consider a planar grain boundary oriented in the microscope such
that it is viewed edge on. This situation may be idealized by the
schematic diagram of figure 3 in which one set of crystal lattice planes
are seen edge on in each of the adjacent grains. In the general case
the orientation of these planes will be different in the two grains,
but they will remain straight and equi-spaced up to the boundary. There
is then a discontinuity. If a thin phase or film is present in the
grain boundary the discontinuity will be a band of finite thickness
whereas if the film is absent the discontinuity will be a line. Very

simply, then, by imaging the lattice planes in adjacent crystalline grains in the vicinity of a grain boundary and examining the continuity of the fringes it is possible to determine whether or not an intergranular phase is present. There are several important consequences of using the fringe imaging method. i) The intergranular phase is detectable irrespective of whether it is crystalline or not, ii) even extremely thin phases, down to the resolution of the microscope, can be detected, and iii) by using the fringe spacing in one of the adjacent grains as a precision scale accurate measurements of the phase thickness may be made.

The stringent conditions required to image the lattice planes as described earlier must be satisfied in both grains simultaneously. Firstly, both grains must be oriented in strongly diffracting conditions for planes whose spacing exceeds the resolution limit of the microscope. The diffraction pattern/objective aperture geometry required is schematically represented in figure 4. Secondly, the grains must both be of a thickness at which the lattice fringes have high contrast. This may be illustrated using the curves of fringe visibility against crystal thickness calculated for silicon nitride. In figure 5 a pair of adjacent grains across a boundary are considered. In one grain the planes are set so that a ten beam systematic row of reflections is formed and the transmitted and 002 beams are used to produce a lattice fringe image. In the other grain again a ten beam systematic row diffraction condition was established but in this case the transmitted and $\bar{1}10$ beams were selected to form the fringe image. From these curves it is clear that certain crystal thicknesses, such as about 800Å, would be

unsuitable for the pair of adjacent grains although the $\bar{1}10$ fringes
would be very strong in one grain. In this particular example the grains
would have to be between about 200Å and 400Å thick in order for the
lattice fringes to be observed on both sides of the boundary.

Such strict requirements pose the problem of how a suitable
boundary is to be selected. In practice, the first step is to translate
and orient the specimen with the microscope operating in the diffraction
mode until two adjacent grains are strongly diffracting. Provided that
the spacings of the diffracting planes exceed the resolution limit the
boundary is viewed in the imaging mode to see whether it is edge on as
required or not. Ideally at this stage the region of the boundary at
the optimum calculated thickness is sought and lattice fringes recorded.
However since foils of pre-determined thicknesses cannot be produced by
the ion-thinning process this region may not be found and sharp,
high-visibility lattice fringes may only be formed in one of the two
adjacent grains.

b) Silicon Nitrides

The loss of high temperature strength of hot pressed silicon
nitride above about 1000°C has been widely attributed to the presence
of a glassy magnesium silicate intergranular phase whose viscosity
rapidly decreases above its softening temperature allowing the silicon
nitride grains to slide past one another. The microstructure envisaged
is schematically illustrated in figure 6. Substantial circumstantial
evidence exists for such a microstructure from Auger electron spectroscopy
of intergranular fracture surfaces, [23,24] from internal friction
measurements [25] and from compression tests where the glass is squeezed

out to the external surfaces [26]. However in each case the information
is obtained from observations sampling a very large number of boundaries
and multiple grain junctions simultaneously and does not indicate
where the silicate phase exists in the microstructure. Specifically to
determine where the glassy phase is located and whether it does exist
as a thin layer surrounding individual grains of silicon nitride or not,
a commercially produced hot-pressed material incorporating MgO as a
fluxing aid (designated HS 130 by its manufacturers) has been examined
using the technique of lattice fringe imaging [27,28]. In this material
it has been estimated from the internal friction measurements and from
volume fraction considerations that the thickness of the layer is
between 50 and 1000Å [25,29]. However it is clear from examining con-
ventional bright-field electron micrographs that intergranular layers
of this thickness are not present. However, to ascertain whether
layers thinner than about 25Å are present using bright-field imaging
is difficult in this material because the electron scattering factors
of all the constituent elements are similar. This is best done by
lattice fringe imaging using the technique described in the previous
section.

Figure 7 is a lattice fringe image of a rotation boundary between
two silicon nitride grains in which one set of the ($10\bar{1}0$) planes is
visible in each grain. In this example the lattice fringes can be
followed right up to the boundary line from either side indicating the
absence of any intergranular phase to within the resolution (~ 3Å) of
the technique. Conceivably a monolayer could still exist at this
boundary, but any thicker layer would be visible. Occasionally a thin

intergranular film is observed but invariably this is seen to be part of
a wedge shaped phase leading from a three or four grain junction. An
example of this is shown in figure 8 where the silicate or second phase
tapers away from the triple grain junction until it is no longer discern-
able. In general the glassy phase is most often to be seen concentrated
at the multiple grain junctions as in figure 9. (The phase contrast
effect due to the evaporated layer of carbon indicates that a phase is
present at the triple junction here and is not merely a hole between
the grains).

As a result of these and many more such observations it can be
concluded that the overall distribution of the silicate phase resembles
the classic findings of C.S. Smith [30] for the distribution of minor
partially wetting phases in metals such as Pb in Cu or beta brass where
the minor phase is located at the tetrahedral interstices formed by
the junction of grains and tapers away from the junction until it is no
longer present. This observed microstructure of course only character-
izes the material as seen at room temperature, whereas the "sand-and-
molasses" model of intergranular sliding depicts the microstructure at
high temperatures. Whether they can be rationalized on the basis of
a temperature dependent wetting by the silicate, as has been
suggested [28], remains to be seen. However, observations of
commercially available specimens that have been quenched after creep
and deformation experiments indicate that their microstructures are
similar to those described here [31].

By using yttria as a fluxing aid in place of the MgO additive
it has been found that the high temperature strength of silicon nitride
can be significantly improved [32]. This improvement has been

attributed to the formation during hot pressing of a refractory phase,
deduced by X-ray diffraction to be a yttrium-silicon oxy-nitride, which
does not soften at about 1000°C as does the magnesium silicate in the
MgO hot-pressed material. However although Rae et al. [33] have
reported that the oxynitride phase is stable to at least 1800°C, the
Y_2O_3 hot-pressed silicon nitride still suffers a high temperature loss
of strength at around 1400°C which indicates that there may be some other
cause for the loss in strength.

The microstructure of a $10^m/o$ Y_2O_3 hot pressed silicon nitride is
illustrated in figure 10, and consists of grains of silicon nitride and
of crystalline silicon-yttrium oxynitride [34]. It is basically similar
to that of the MgO fluxed materials with the oxy-nitride phase, as with
the magnesium silicate phase above, being heterogeneously distributed
and concentrated principally at the multiple grain junctions. (The
silicon yttrium oxynitride phase has higher contrast than the magnesium
silicate on account of the larger electron scattering factor of the
yttrium atoms). The dihedral angles formed by the oxynitride phase
indicate that it does not penetrate between the silicon nitride grains
to form a continuous intergranular film.

However, in determining the extent of the oxynitride phase an
additional phase not identified by X-ray diffraction analysis was
detected [34]. This is an intergranular phase between the silicon
nitride grains and the silicon-yttrium oxynitride grains and should
properly be referred to as an interphase phase. Although it can be
seen in thin regions of the specimen by conventional bright field imaging,
its presence is best revealed by lattice fringe imaging as in figure 11.

As with the previous examples presented here there is no way of establishing whether or not this interphase phase is crystalline. Its absence in the X-ray diffraction data can be accounted for by its small volume fraction in the microstructure deduced from the narrowness of the phase in the boundaries.

The unexpected finding of an intergranular phase suggests that it may be the origin of the strength degradation exhibited at high temperatures. However recent X-ray spectroscopy analyses using a STEM facility [35,36] of the silicon-yttrium oxynitride phase from regions as small as 150Å across imply that melting below 1800°C caused by impurity alloying may be an alternative explanation [36].

ii) Phase Transformations in Silicon Carbide.

The polytypic phase transformations in silicon carbide have long been of scientific interest to crystallographers and physicists concerned with the phenomenon of polytypism. In recent years however the interest in these transformations has broadened with the developments aimed at demonstrating that silicon carbide is a viable high temperature engineering material.

When silicon carbide materials, sintered or hot-pressed from β (cubic stacking) powders, are held at high temperatures ($\gtrsim 1800°C$) two processes related to polytypism occur. One is the phase transformation from the cubic stacking form, β, to any of the hexagonal or rhombohedral forms (denoted here for the sake of brevity as α), and the other is an exaggerated grain growth [37]. To investigate the mechanism of the phase transformation two types of silicon carbide have been studied, the boron doped and sintered material produced by

General Electric [38] and the reaction sintered material known as REFEL silicon carbide [39]. Whilst both types of material have been extensively studied very little is known about the mechanism of the transformation itself although on account of its morphology it has been likened to that of a massive transformation [40].

The microstructure of the partially transformed boron sintered carbide is that of long lath shaped grains each consisting of parallel intergrowths of β, twinned β and α stacked regions [41]. The intergrowths are also lath shaped and almost without exception are parallel to and bounded by the same close packed plane in the crystal. A previously published lattice fringe imaging study [41] reveals that the scale of the intergrowth can be extremely fine with the laths being as small as one unit cell wide. Despite this complexity however, a striking simplicity of the microstructure is that the β and α stacked regions extend completely across the grains from one boundary to another. As a result the only transformation interface that can be studied is the bounding close packed plane of the laths, which might be termed the non-glissile interface. To observe the "glissile" interface another type of silicon carbide is clearly needed. Reasoning that the boron sintered material is too pure to allow impurity drag to peg the "glissile" interface in the middle of the grain, the less-pure reaction sintered REFEL material was chosen [42].

Whether impurity pinning is the cause or not, the "glissile" interface can be observed in the REFEL material. Figure 12 is a low magnification view of a grain of the material oriented with the beam

parallel to [11$\bar{2}$0] so that the close packed planes are seen edge on.
By selected area electron diffraction analysis the light areas are
found to be regions of cubic stacking, whereas the dark areas are
regions of α. Even at this relatively low magnification the irregular
nature of the "glissile" boundary is obvious together with the smooth
character of the "non-glissile" ones. The details of the interface
are seen at higher magnification in the lattice fringe image of figure
13 where the 15.2Å periodicity of the (0001) planes in the α-6H
polytype has been imaged. Due to the imaging conditions used only
those regions with the α-stacking display fringes. The irregular fringe
terminations represent the morphology of the glissile interface, and the
presence of one fringe high steps strongly suggest that the inter-face
advances by the progression of successive unit cell ledges across the
material [42]. Such an interpretation is in keeping with the observation
that the lath shaped regions of α and β are bounded by the close packed
planes.

iii) Crystal Structure Refinement

One of the more dramatic applications of high resolution electron
microscopy is in the refinement of crystal structure, particularly in
elucidating the fine structure variations due to faulting, stacking
disorders and unit cell scale twinning, all of which can be difficult
if not impossible to determine from conventional X-ray data [5].
This type of work, in which the details of the structure and the
projection of the atoms are seen directly, has been restricted until
now to structure analysis of the niobium-oxide class of oxides [43],
the tungsten bronzes and some minerals [5]. These are particularly

suitable materials since they have rather open structures with large interatomic distances and contain relatively heavy elements, so giving rise to strong contrast.

Despite the striking structure images obtained from these materials the technique of structure imaging has only just begun to be applied to materials of interest to the ceramicist. Primarily this is because industrial ceramics generally have close packed structures, and so the information sought is close to the resolution limitations of the microscope making it much more difficult to obtain. Nevertheless useful crystallographic information about ceramics can be obtained as the following illustrations, drawn from a study of the "X" phase, demonstrates.

One important aspect of structure imaging is that under suitable circumstances the image obtained may be intuitively interpreted in terms of the actual atomic positions, and so atoms observed around crystal defects are seen as clearly as those in perfect regions of the crystal. The appropriate conditions must be ascertained by computation, but it is found that for specimen thicknesses of approximately 50Å at an objective lens defocus setting of about 900Å the image corresponds directly to the projected charge density in the crystal [14].

(a) X Phase.

The X phase is one of a series of phases that exist in the Si-Al-O-N system and is usually an undesirable phase in the fabrication of the β' Sialon [44]. In the literature it has been variously referred to as the "J", "X" and "Oyama" phase reflecting the uncertainty in its

composition and crystal structure [44]. To date three different unit
cells have been assigned and each belongs to a different symmetry
group [44-46]. Whilst it may possibly exist as more than one crystal
structure a number of basic crystallographic questions about the phase
can be quite simply answered by structure imaging. Amongst these are,
what are the angles between the planes whose spacings have been
determined from the X-ray powder patterns; are some of the X-ray
reflections observed caused by fine scale ordering of faults or micro-
twins; what fault displacements are present?

Figure 14 is a structure image of a very thin region near the edge
of the foil of a small grain of "X" phase obtained using 21 diffracted
beams in the configuration of figure 2(b) and projected down a two-fold
zone axis. In this very perfect region the translational periodicity
of the structure is evident and indicates that the basic repeat unit
in this projection is a parallelogram with a principal interplanar
angle of 80°. The lighter regions represent channels of lower electrical
potential than the surrounding areas.

An intriguing aspect of the electron diffraction patterns taken in
this orientation is that they can be indexed equally well on the basis
of a microstructure containing a high density of microtwins or on the
basis of a periodic faulting structure in which some of the individual
unit cells are displaced relative to one another by one third of a
translation vector. Although features characterisitic of both faults
and microtwins are observed by conventional microscopy they are
generally on such a fine scale that they cannot be distinguished.
Figure 15 is taken from an adjacent equally thin but faulted region

to that of figure 14 and in this case an isolated fault having a projected displacement of $T/3$ where T is a lattice translation vector can be seen. (Since the unit cell has yet to be agreed upon, T is the translation vector that repeats the lattice in the structure image). No evidence for twinning is found in these and similar structure images indicating that faulting is an important crystallographic feature in this material.

These preliminary examples of structure images of a ceramic demonstrate that structure imaging can supplement crystal structure analysis, particularly when based on X-ray powder diffraction methods, and as they were also obtained from ion-thinned material, indicate that the technique can be applied to the study of ceramics conventionally prepared.

ACKNOWLEDGEMENT

REFERENCES

1. D. J. H. Cockayne, I.L.F. Ray and M. J. Whelan, "Investigations of Dislocation Strain Fields Using Weak Beams", Phil. Mag. 20, 1265-1270 (1969).

2. M. J. Goringe, E. A. Hewat, C. J. Humphreys and G. Thomas, "Defect Contrast and Resolution in High Voltage Electron Microscopy", Proc. Fifth European Congress on Electron Microscopy, Manchester, 1972, 538-539.

3. R.S.M. Revell, "Philips Analytical Equipment Bulletin", N. V. Philips, Eindhoven, The Netherlands (1973).

4. J. W. Menter, "The Direct Study by Electron Microscopy of Crystal Lattices and Their Imperfections", Proc. Roy. Soc. A326, 119-135 (1956).

5. See for instance, "Electron Microscopy in Mineralogy", edited H.-R. Wenk, Springer-Verlag, New York, (1976).

6. M. Born and E. Wolf, "Principles of Optics", Pergamon Press, London (1964).

7. J. M. Cowley, "Diffraction Physics", North-Holland, Amsterdam (1975).

8. R. D. Heidenreich, "Fundamentals of Transmission Electron Microscopy" Wiley-Interscience, New York, (1964).

9. W. C. T. Dowell, "Das Elektronenmikroskopische Bild von Netzkenenscharen und Sein Kontrast" Optik, 20 (11), 535-568, (1963).

10. O. Scherzer, "The Theoretical Resolution Limit of the "Electron Microscope", J. App. Phys., 20, 20-29 (1949).

11. M. A. O'Keefe, Ph.D. Thesis, University of Melbourne, 1975.

12. J. G. Allpress and J. V. Sanders, "The Direct Observation of the Structure of Real Crystals by Lattice Imaging", J. App. Cryst., 6, 165-190 (1973).

13. J. M. Cowley and S. Iijima, "Electron Microscope Image Contrast for Thin Crystals", Zeit, Natur. 27a, 445-451 (1972).

14. D. F. Lynch, A. F. Moodie and M. A. O'Keefe, "n-Beam Lattice Images. V. Use of the Charge Density Approximation in the Interpretation of Lattice Images", Acta. Cryst., A31, 300-307 (1975).

15. J. M. Cowley, "The Electron-Optical Imaging of Crystal Lattices", Acta. Cryst., 12, 367-375 (1959).

16. H. Hashimoto, M. Marnami and T. Naiki, "Dynamical Theory of Electron Diffraction for the Electron Microscopic Image of Crystal Lattices", Phil. Trans., 253, 459-489 (1961).

17. A. J. F. Metherell, "Diffraction of Electrons by Perfect Crystals", in "Electron Microscopy in Materials Science", edited E. Ruedl and U. Valdre, Commission of the European Communities, Luxemborg (1977).

18. M. A. O'Keefe, "n-Beam Lattice Images. IV. Computed Two-Dimensional Images", Acta Cryst., A29, 389-401 (1973).

19. M. A. O'Keefe and J. V. Sanders, "n-Beam Lattice Images. VI. Degradation of Image Resolution by a Combination of Incident Beam Divergence and Spherical Aberration", Acta. Cryst., A31, 307-310 (1975).

20. J. G. Allpress, E. A. Hewat, A. F. Moodie and J. V. Sanders, "n-Beam Lattice Images. I. Experimental and Computed Images from $W_4Nb_{26}O_{77}$", Acta Cryst., A28, 528-536 (1972).

21. D. F. Lynch and M. A. O'Keefe, "n-Beam Lattice Images. II. Methods of Calculation", Acta Cryst., A28, 536-548 (1972).

22, G. R. Antis, D. F. Lynch, A. F. Moodie and M. A. O'Keefe, "n-Beam Lattice Images. III. Upper Limits of Ionicity in $W_4Nb_{26}O_{77}$", Acta Cryst. A29, 138-147 (1973).

23. R. Kossowsky, "The Microstructure of Hot-Pressed Silicon Nitride", J. Mater. Sci., $\underline{8}$ (11), 1603-1615 (1973).

24. B. D. Powell and P. Drew, "The Identification of a Grain Boundary Phase in Hot-Pressed Silicon Nitride by Auger Electron Spectroscopy", J. Mater. Sci., $\underline{9}$ (11), 1867-1870 (1974).

25. D. R. Mosher, R. Raj and R. Kossowsky, "Measurement of Viscosity of the Grain Boundary Phase in Hot-Pressed Silicon Nitride", J. Mater. Sci., $\underline{11}$ (1), 49-53 (1976).

26. P. Spencer, M. S. Thesis, University of California, Berkeley (1977).

27. D. R. Clarke, "Direct Observations of Lattice Planes at Grain Boundaries in Silicon Nitride", in "Nitrogen Ceramics", edited F. Riley, In Press.

28. D. R. Clarke and G. Thomas, "Grain Boundary Phases in a Hot-Pressed MgO Fluxed Silicon Nitride", J. Am. Ceram. Soc. 1977, In Press.

29. F. F. Lange, "Non-Elastic Deformation of Polycrystals with a Liquid Boundary Phase", in "Deformation of Ceramic Materials", edited R. C. Bradt and R. E. Tressler, Plenum Pub. Co., New York (1974).

30. C. S. Smith, "Grains, Phases and Interfaces: An Interpretation of Microstructure", Trans. A.I.M.E., $\underline{175}$, 15-51 (1948).

31. D. R. Clarke, unpublished work.

32. G. E. Gazza, "Effect of Yttria Additions on Hot-Pressed Si_3N_4", Amer. Ceram. Soc. Bull., $\underline{54(a)}$, 778-781 (1975).

33. A. W. J. M. Rae, D. P. Thompson, N. J. Pipkin and K. H. Jack, "The Structure of Yttrium Silicon Oxynitride and Its Role in the Hot-Pressing of Silicon Nitride with Yttria Additions", in "Special Ceramics 6", edited P. Popper, British Ceramic Research Association, p 347-360 (1975).

34. D. R. Clarke and G. Thomas, "Microstructure of Y_2O_3 Fluxed Hot-Pressed Silicon Nitride", J. Am. Ceram. Soc., In Press 1977.

35. R. H. Geiss and D. R. Clarke, "Combined Analytical and High Resolution Microscopy-A Case Study", 35th Ann. Proc. Electron Microscopy Soc. Am., ed. G. W. Bailey, 146-147 (1977).

36. R. H. Geiss and D. R. Clarke, In preparation.

37. See for instance papers in "Silicon Carbide - 1973", edited R. C. Marshall J. W. Faust and C. E. Ryan, University of South Carolina Press (1974).

38. S. Prochazka, "Sintering of Silicon Carbide", 239-250, in "Ceramics for High Performance Applications", edited J. E. Burke, A. E. Gorum and R. N. Katz, Brook Hill, Mass. (1974).

39. C. W. Forrest, P. Pennedy and J. V. Shennan, "The Fabrication and Properties of Self-Bonded Silicon Carbide Bodies", in "Special Ceramics 5", edited P. Popper, British Ceramic Research Association (1972).

40. S. Shinozaki and K. R. Kinsman, "Influence of Structure on Morphology in Polycrystalline Silicon Carbide", in "Ceramic-Microstructures - 76", edited R. M. Fulrath and J. A. Pask, Westview, Boulder (1977).

41. G. Thomas, D. R. Clarke and O. Van der Biest, "The Impact of Transmission Electron Microscopy in Ceramics", in "Ceramic Microstructures - 76", edited R. M. Fulrath and J. A. Pask, Westview, Boulder (1977).

42. D. R. Clarke, "The Morphology of the Transformation Interface in Reaction Sintered Silicon Carbide", J. Am. Ceram. Soc., In Press (1977).

43. S. Iijima, "High Resolution Electron Microscopy of Crystal Lattice of Titanium-Niobium Oxide", J. App. Phys., 42 (13), 5891-5893 (1971).

44. K. H. Jack, "Review: Sialons and Related Nitrogen Ceramics", J. Mater. Sci., 11 (5), 1135-1158 (1976).

45. P. Drew and M. H. Lewis, "The Microstructures of Silicon Nitride/Alumina Ceramics", J. Mater. Sci., $\underline{9}$ (11) 1833-1838 (1974).

46. E. Gugel, I. Petzenhauser and A. Fickel,

Powder Met. Int., $\underline{7}$ (1), 66-73 (1975).

FIGURE CAPTIONS

FIG. 1. Schematic Ray diagram illustrating the formation of a two

beam lattice fringe image in an electron microscope.

FIG. 2. Configuration of the electron diffraction pattern, outline of

the objective aperture and the position of the optic axis in the

back focal plane for a) two-beam tilted-illumination lattice fringe

imaging, b) many-beam axial-illumination structure imaging and,

c) many-beam tilted-illumination dark field structure imaging.

Schematic.

FIG. 3. Idealized projection of a grain boundary region containing a

second phase at the boundary. The boundary is seen edge on as

are one set of crystal lattice planes in the two adjacent grains

A and B.

FIG. 4. Objective aperture, optic axis and diffraction pattern con-

figuration in the back focal plane of the objective for imaging

one set of lattice fringes in two grains on either side of a

grain boundary. Schematic. g_1 is the fundamental reflection from

one grain and g_2 from the second grain.

FIG. 5. Ten-beam dynamical electron diffraction computation of lattice

fringe visibility versus thickness of the crystalline grains. The

full line refers to visibility of fringes formed in one grain

from the recombination of the transmitted beam and the $\bar{1}10$

diffracted beam, and the dashed line represents the visibility of

fringes in the adjacent grain in which the transmitted and 002

diffracted beams have been recombined. A tilted illumination

configuration corresponding to figure 2a was assumed.

FIG. 6. The "sand and molasses" microstructure envisaged for the structure of hot-pressed silicon nitride at high temperatures; grains of silicon nitride are surrounded and separated by a continuous layer of second phase shown here by the black lines.

FIG. 7. Lattice fringe image of a rotation boundary in a hot pressed silicon nitride. The lattice fringes are seen to be continuous right up to and on either side of the boundary where there is a line discontinuity indicating an absence of any intergranular phase. The $(10\bar{1}0)$ lattice spacing is 6.5Å.

FIG. 8. Lattice fringe image close to a three-grain junction. A thin intergranular phase is revealed which decreases in thickness away from the 3-grain junction until it cannot be discerned. Note that the wedge shape of the intergranular phase is determined by the $(10\bar{1}0)$ planes in the two adjacent silicon nitride grains. Hot pressed silicon nitride.

FIG. 9. A three-grain junction in a MgO-fluxed hot-pressed silicon nitride. The lattice fringes in the top and lower right grains clearly show that the intergranular phase is located at the grain junction, A, with a very thin film (~8Å) leading from it between the two grains. Although the lower left grain is out of contrast the Moire fringes, B, indicate that it is crystalline too. $(10\bar{1}0)$ spacing is 6.5Å.

FIG. 10. Low magnification bright field electron micrograph illustrating the microstructure of a Y_2O_3-fluxed and hot-pressed silicon nitride. The silicon-yttrium oxynitride second phase (black) is located principally at the multiple silicon nitride grain junctions (arrowed).

FIG. 11. A lattice fringe electron micrograph revealing the existence of a thin (≤ 70Å) intergranular phase between a silicon nitride grain (left) and a silicon-yttrium oxy-nitride grain (right). The $(10\bar{1}0)_{Si_3N_4}$ spacing is 6.5Å.

FIG. 12. Low magnification bright-field electron micrograph of a reaction sintered silicon carbide. The light regions are, by selected area electron diffraction, cubic (3C) and the dark regions hexagonal (α) silicon carbide. The smooth transformation interface termed here as the "non-glissile" interface is parallel to the (0001) plane. The interfaces not parallel to this are seen to be mainly irregular and are referred to here as the "glissile" transformation interface.

FIG. 13. High magnification lattice fringe micrograph of a "glissile" transformation interface. The fringes are parallel to (0001) and have a spacing of 15.2Å denoting those regions of 6H silicon carbide. The cubic (3C or β) regions have no fringes. The irregular interface is seen to be stepped with steps one fringe high, suggesting that the interface advances by the progression of successive unit-cell high ledges across the material.

FIG. 14. n-beam axial illumination structure image of X-phase. The darker regions probably represent regions of higher projected charge density, in this image taken in a very thin region of the foil. The translational periodicity of the structure and the principle angle between the basis vectors are evident.

FIG. 15. n-beam axial-illumination structure image of an adjacent thin region of X-phase. A fault having a projected displacement of one-third of the translational periodicity is arrowed. (This can best be seen by viewing the figure obliquely along the rows inclined to the fault line). Basic crystallographic information can thus be seen directly.

XBL 7 7 7-5749A

FIG. 1

(a)

(b)

(c)
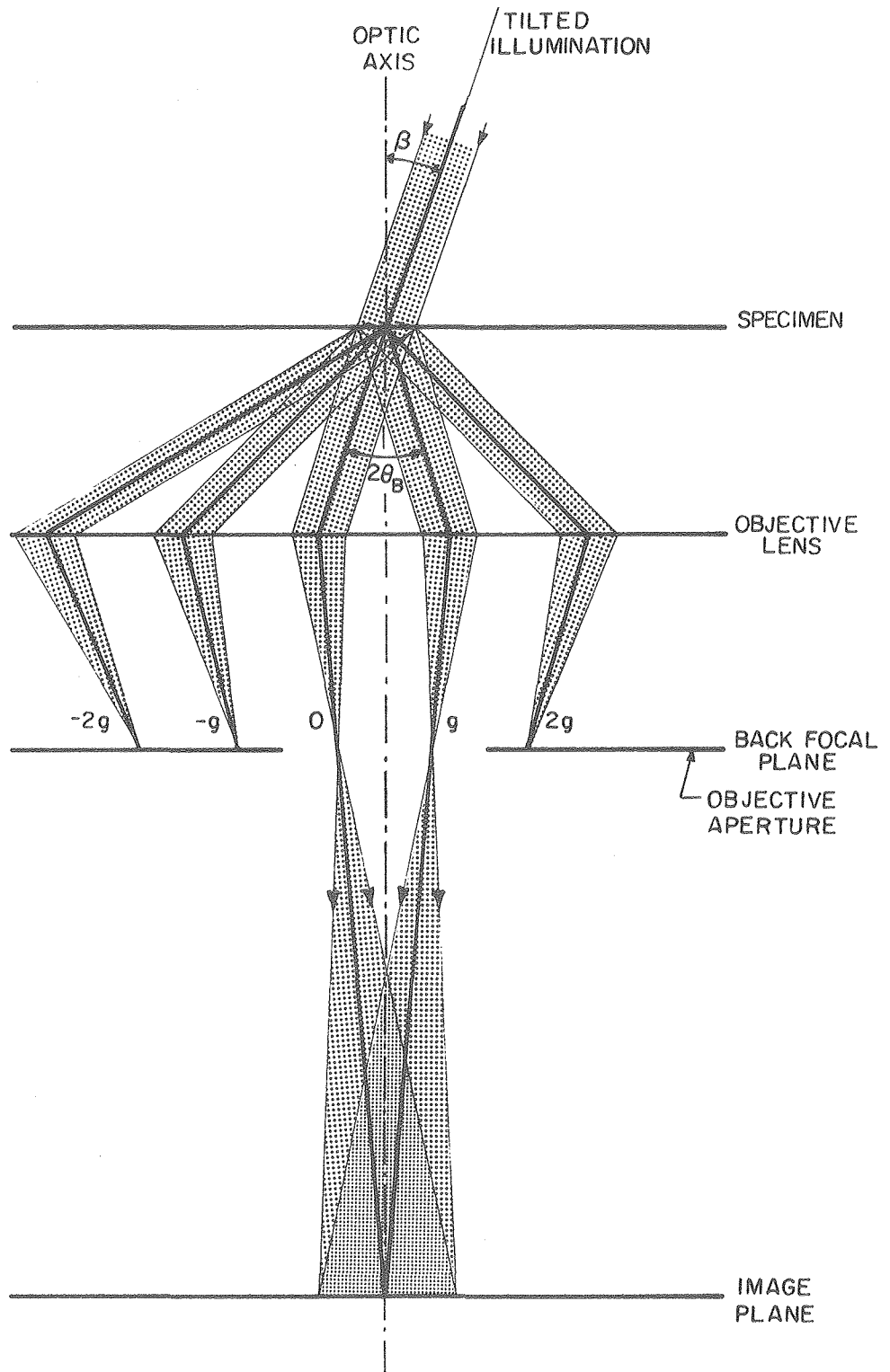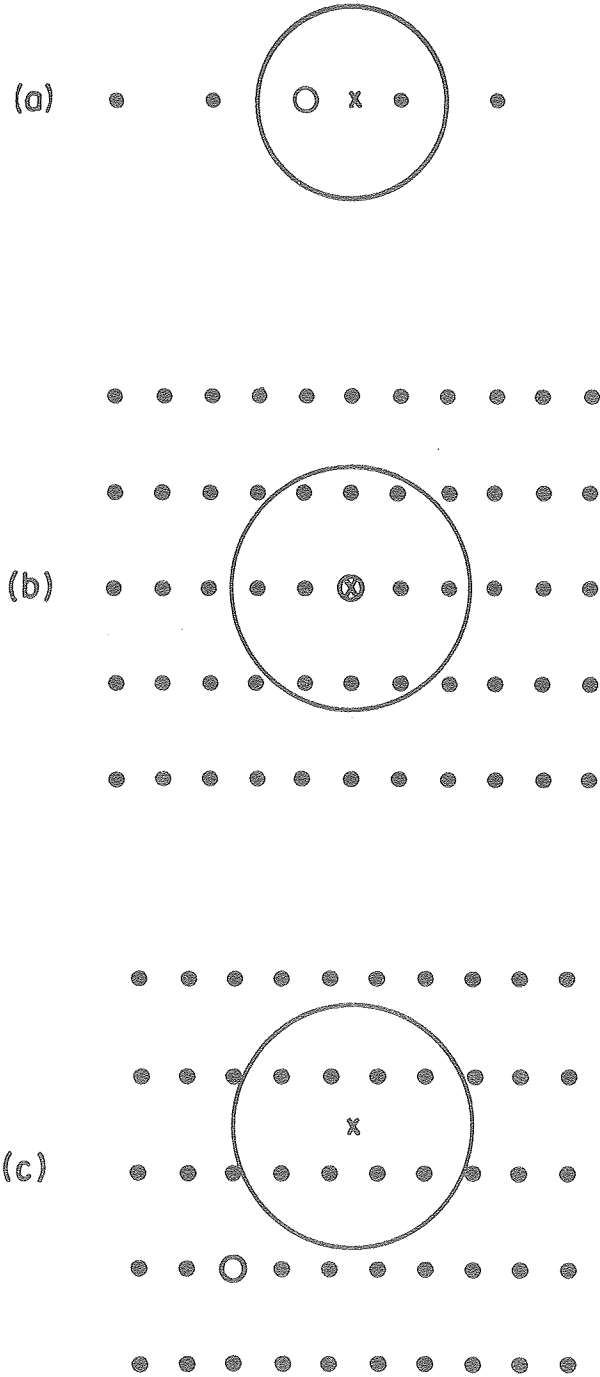
x OPTIC AXIS
O TRANSMITTED BEAM

XBL 778-5880

FIG. 2

GRAIN A

↑

GRAIN BOUNDARY
PHASE
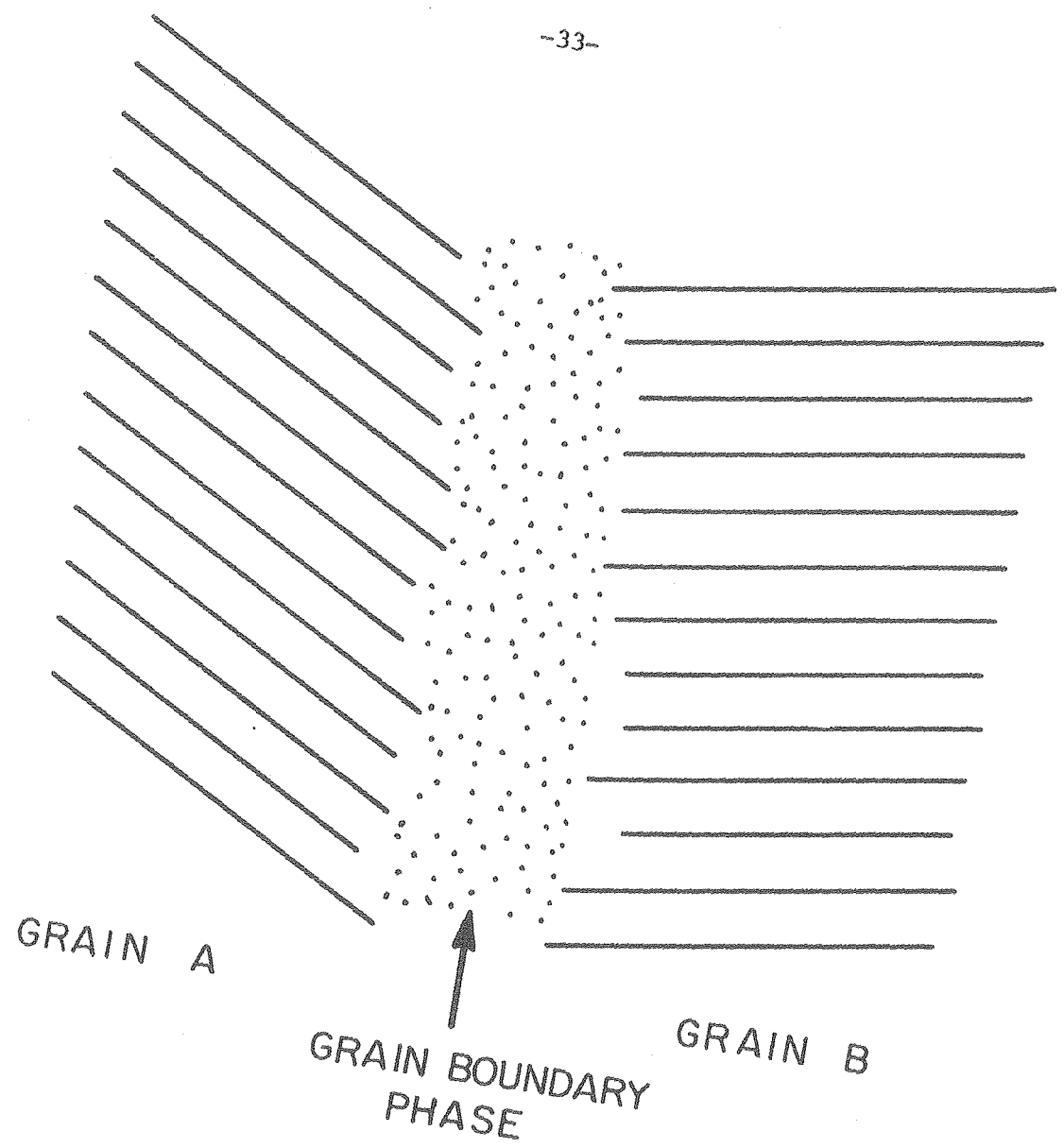
GRAIN B

PROJECTION LOOKING DOWN THE GRAIN BOUNDARY.
THE CRYSTAL LATTICE PLANES ARE SEEN EDGE ON.

XBL 7611-7785

FIG. 3

$3g_{2_0}$

$2g_{2_0}$

g_{2_0}

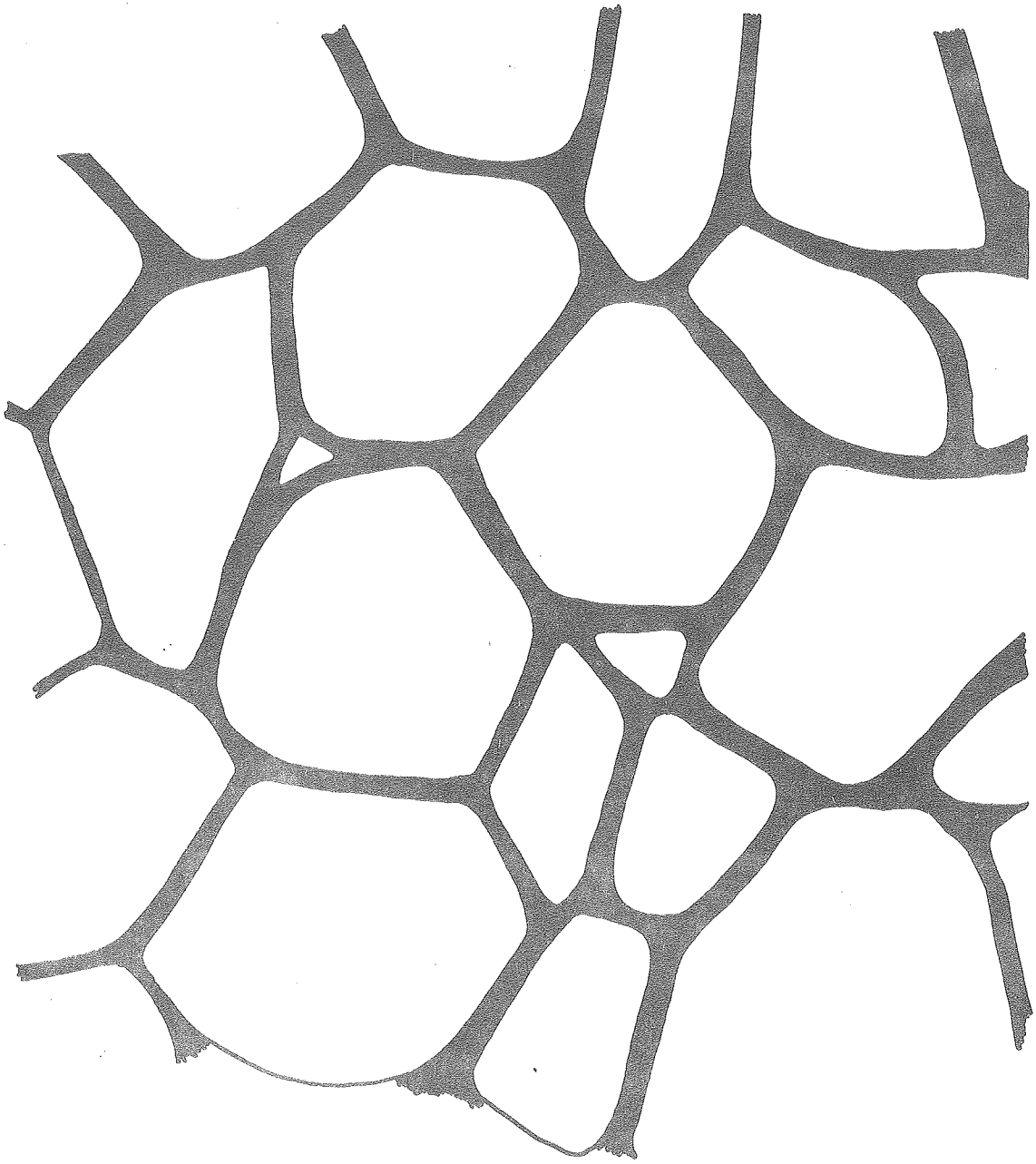$-g_1$ $\otimes$ g_1 $2g_1$
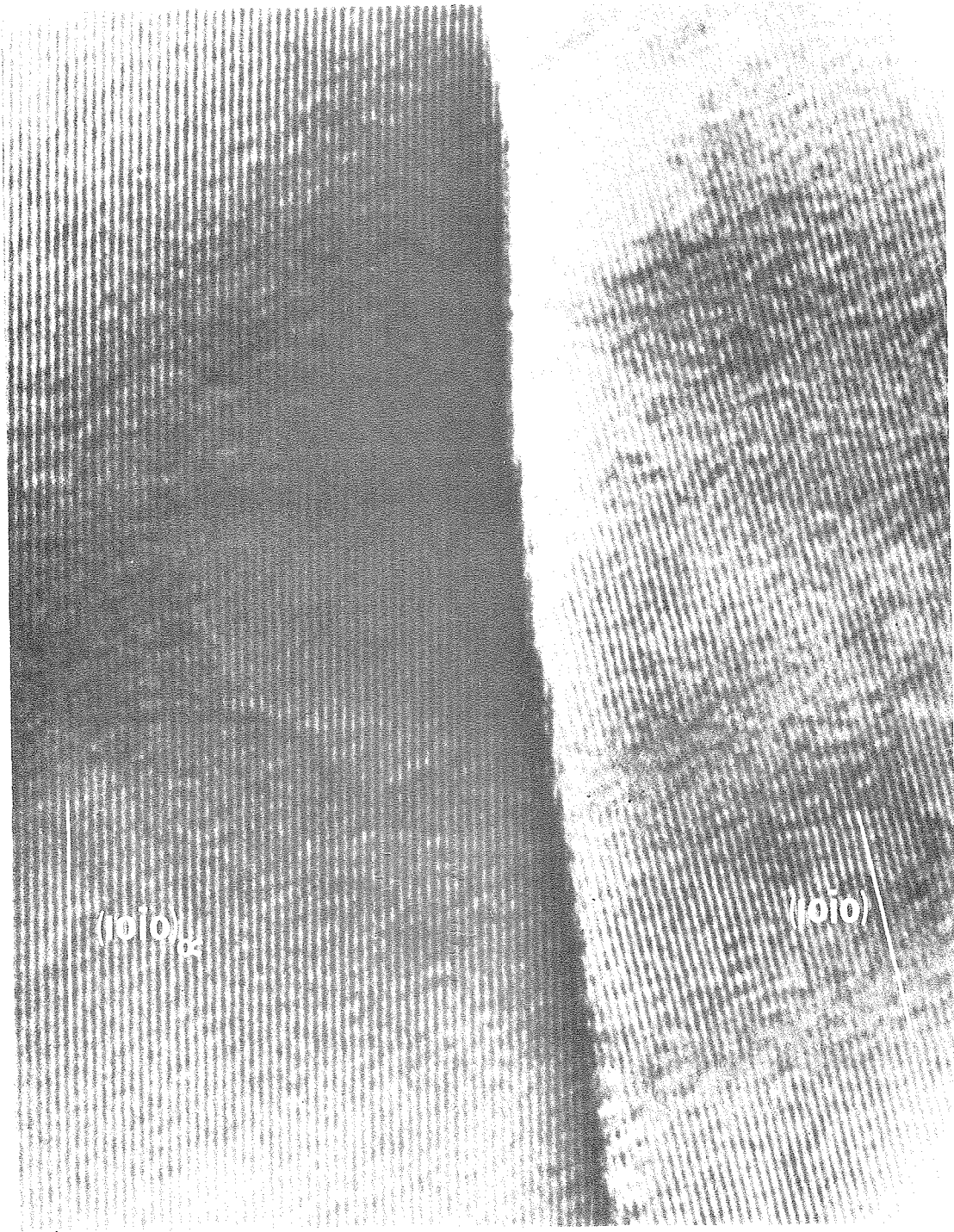
$\circ$

$-2g_{2_0}$

$-3g_{2_0}$
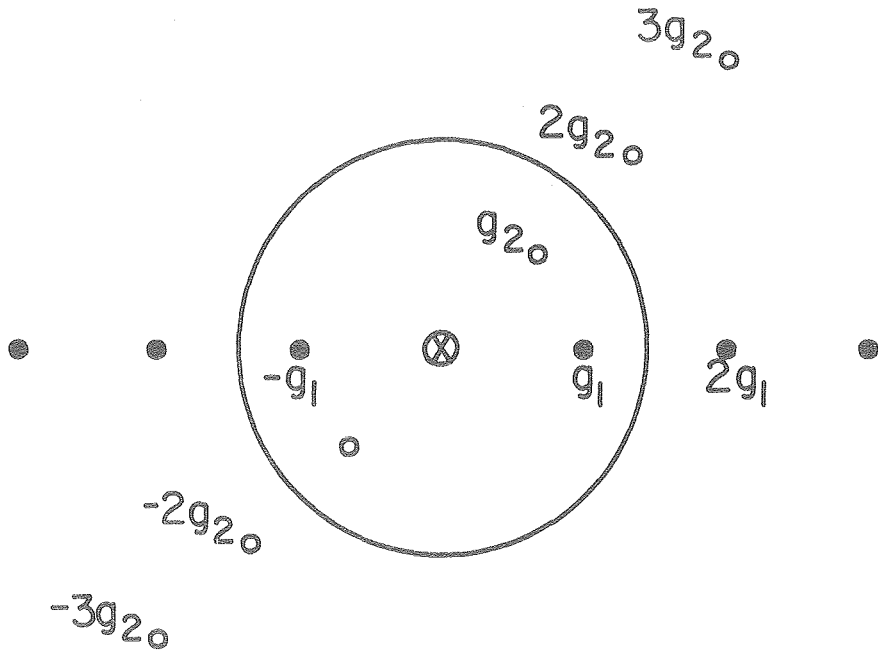
XBL778-5993

FIG. 4
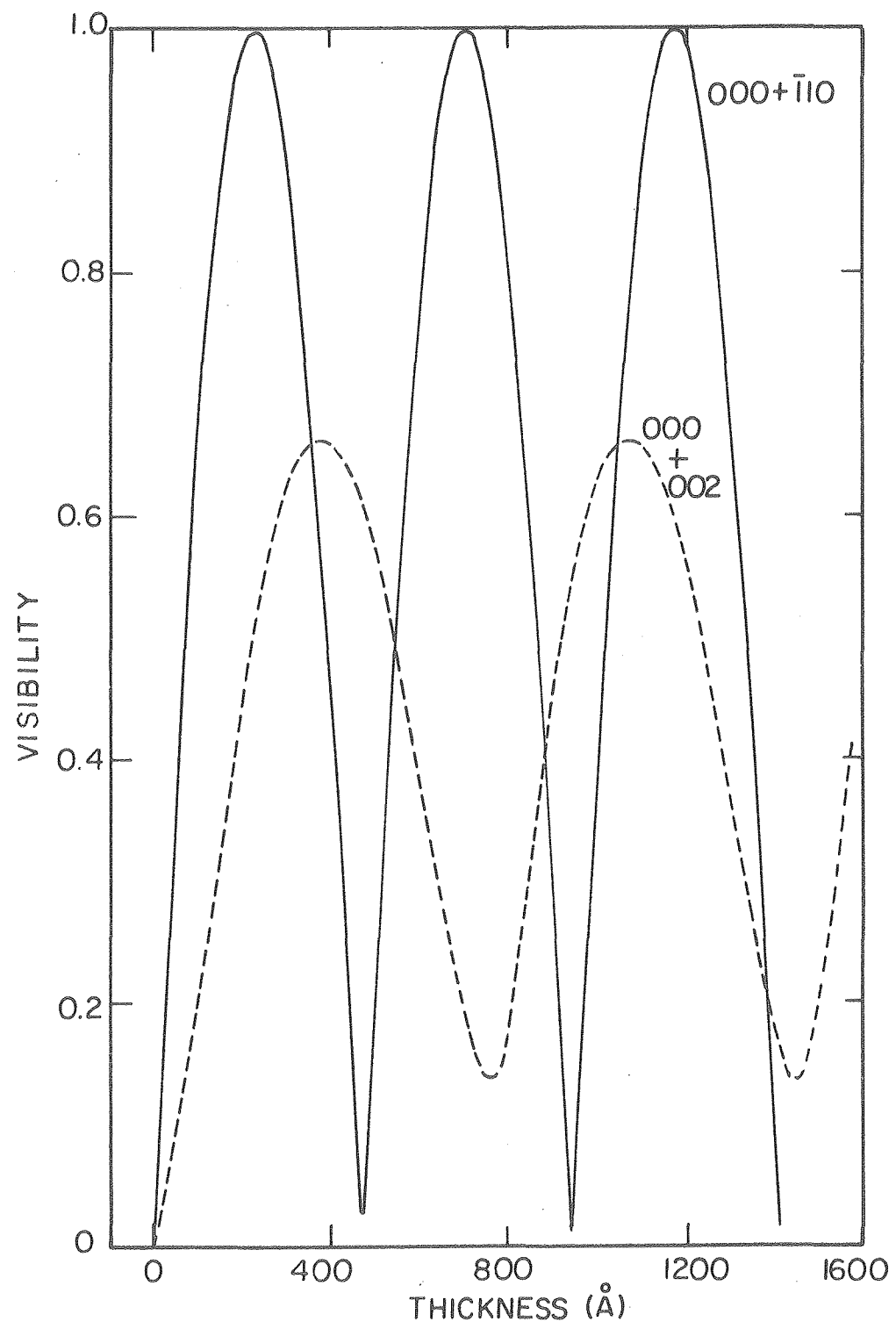
FIG. 5

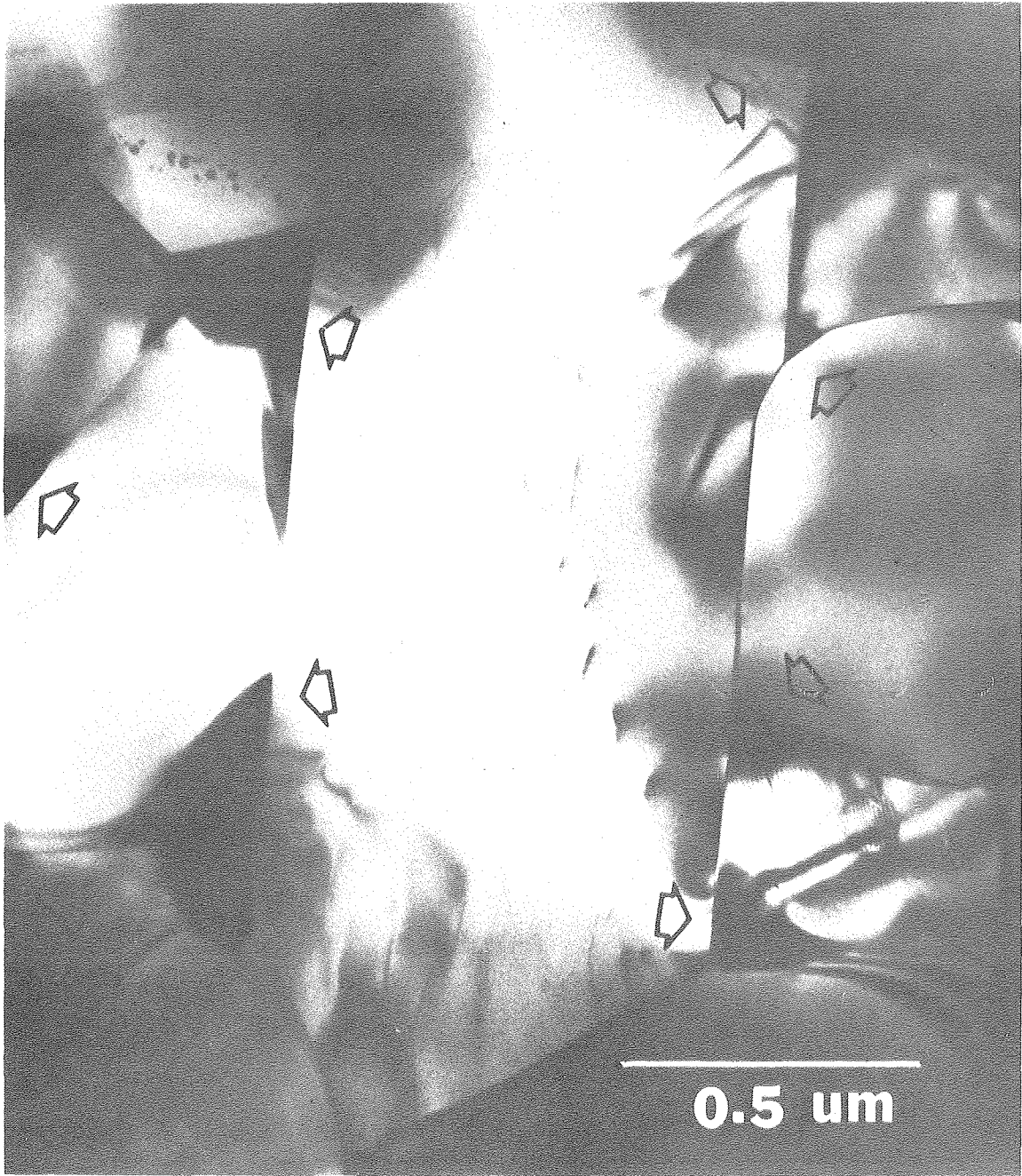SAND AND MOLASSES MODEL
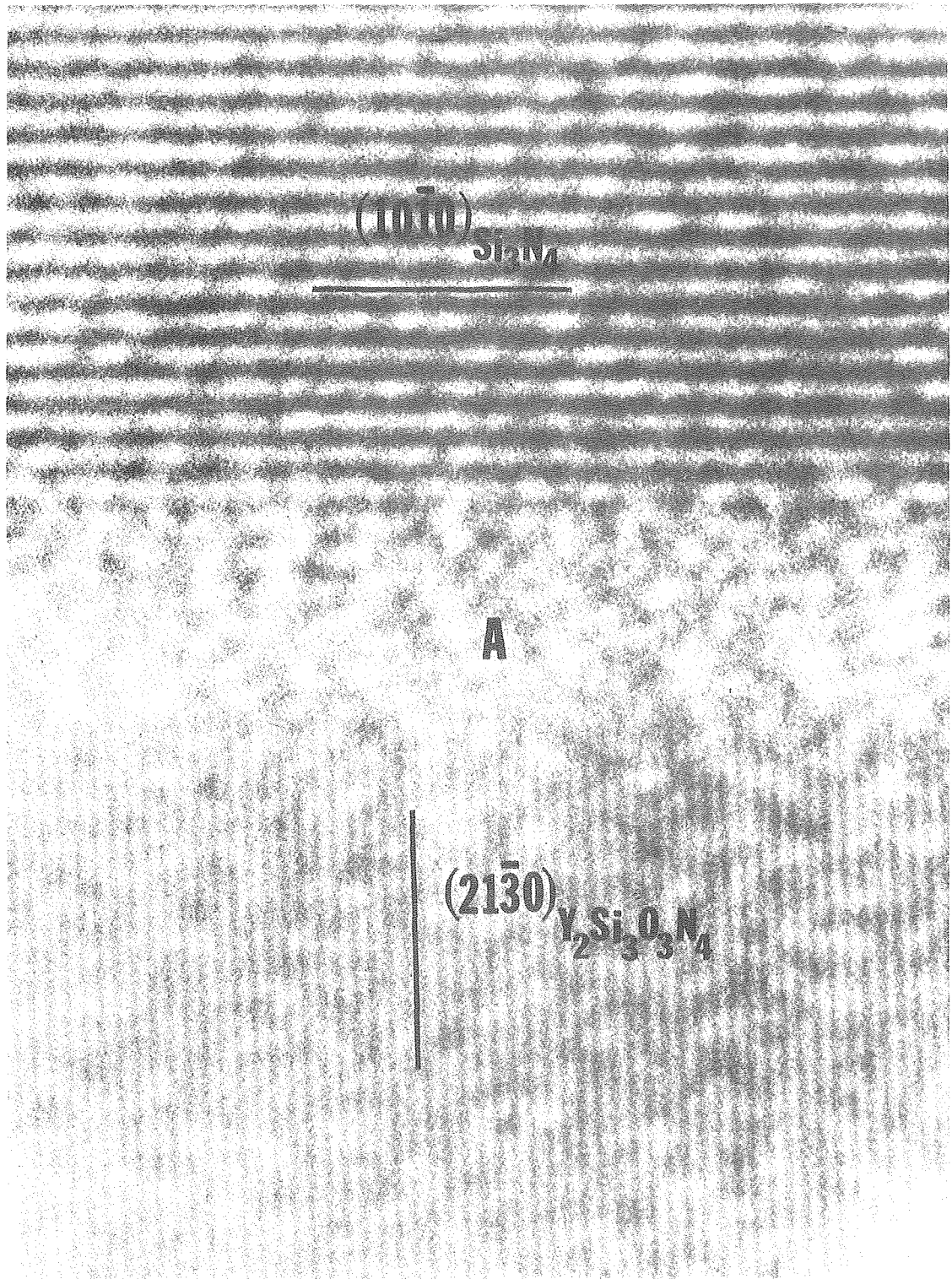
XBL 7611-7784

FIG. 6

XBB 7610-9736

FIG. 7
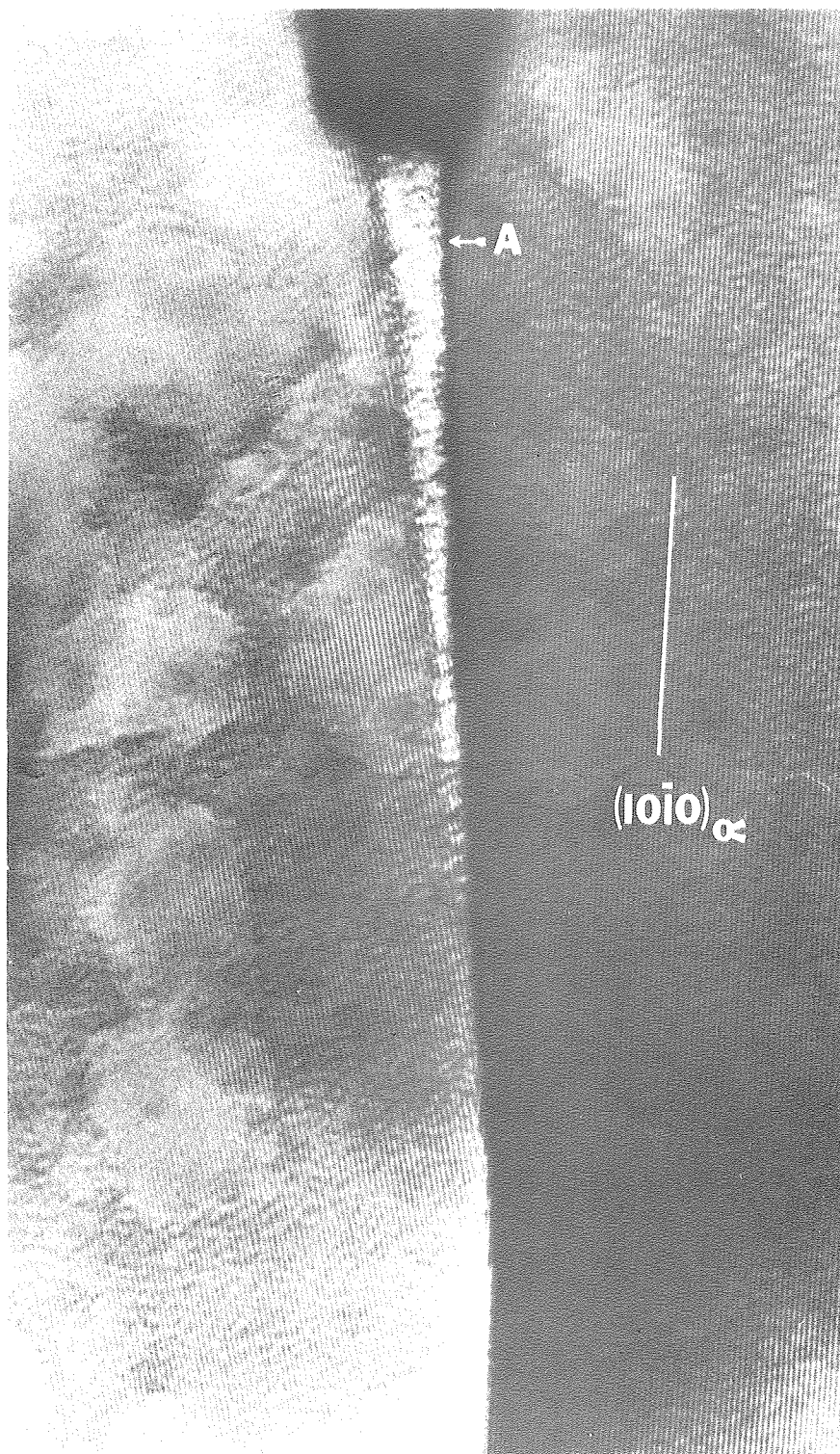
XBB 7610-9732

FIG. 8
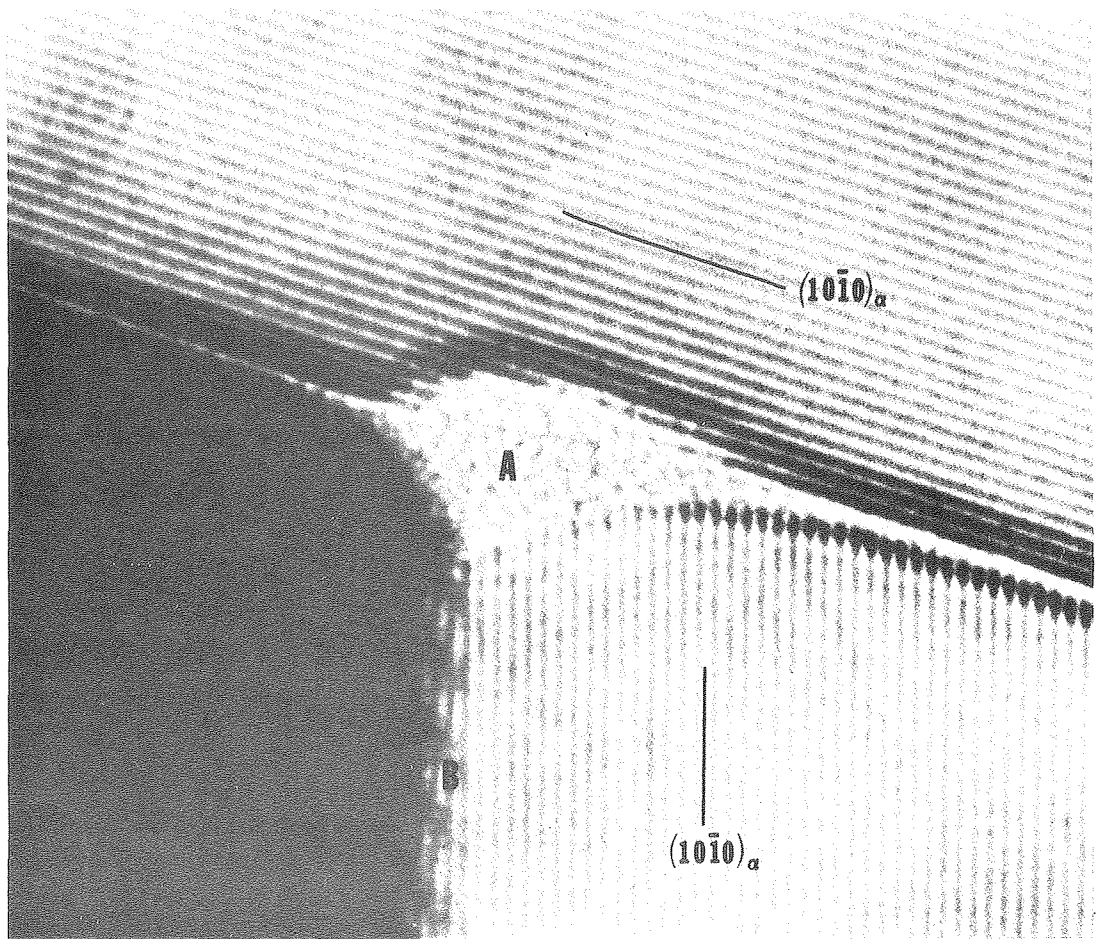
XBB 769-8516

FIG. 9

XBB 772-778

FIG. 10

$(11\bar{1}0)_{SiRN}$

A

$(21\bar{3}0)_{Y_2Si_3O_3N_4}$

XBB 778-7595

FIG. 11

(111)

2500 Å

777-7362A

FIG. 12

6 H

3 C

6 H
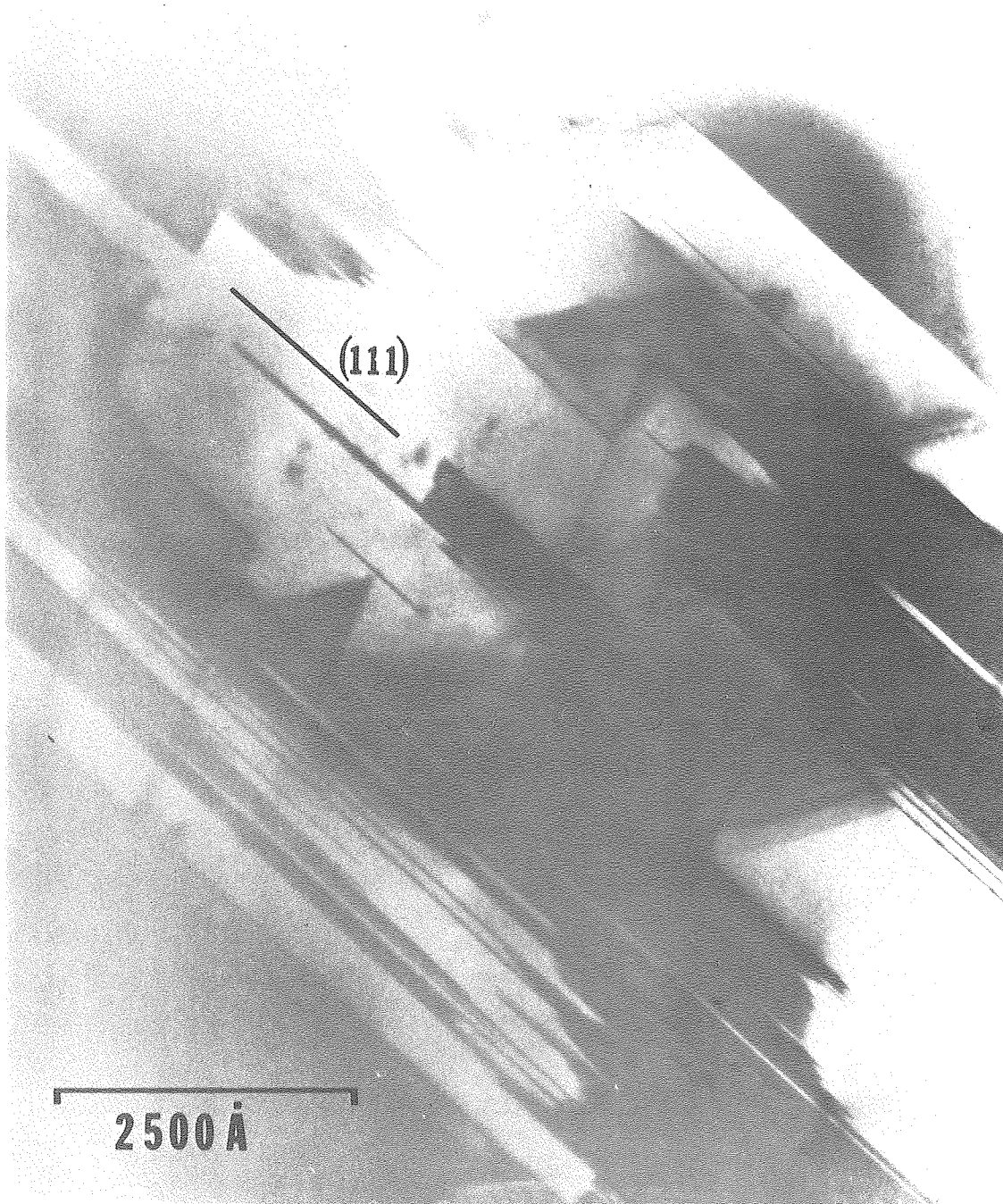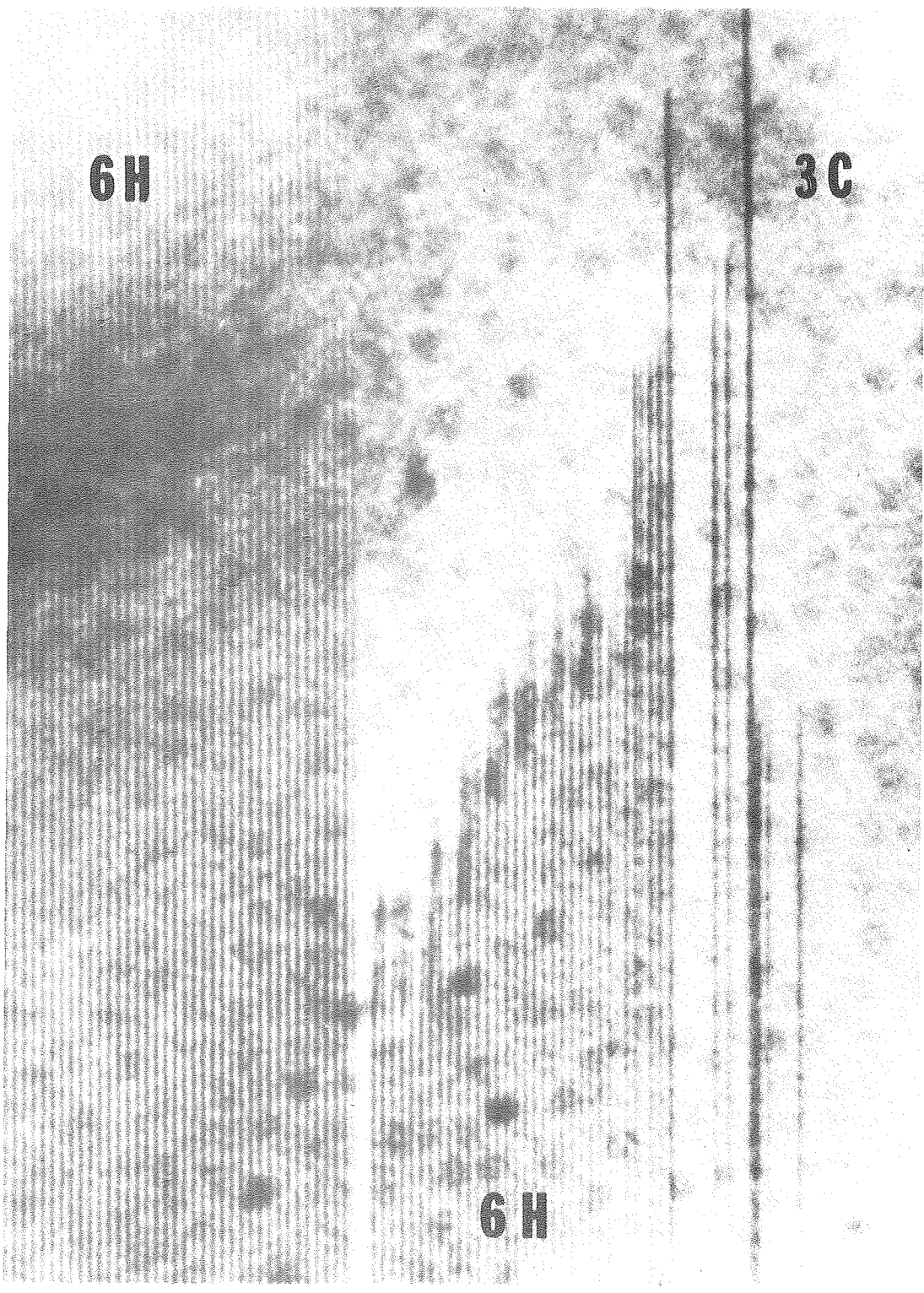
XBB 778-7364

FIG. 13

X Phase

7·8 A
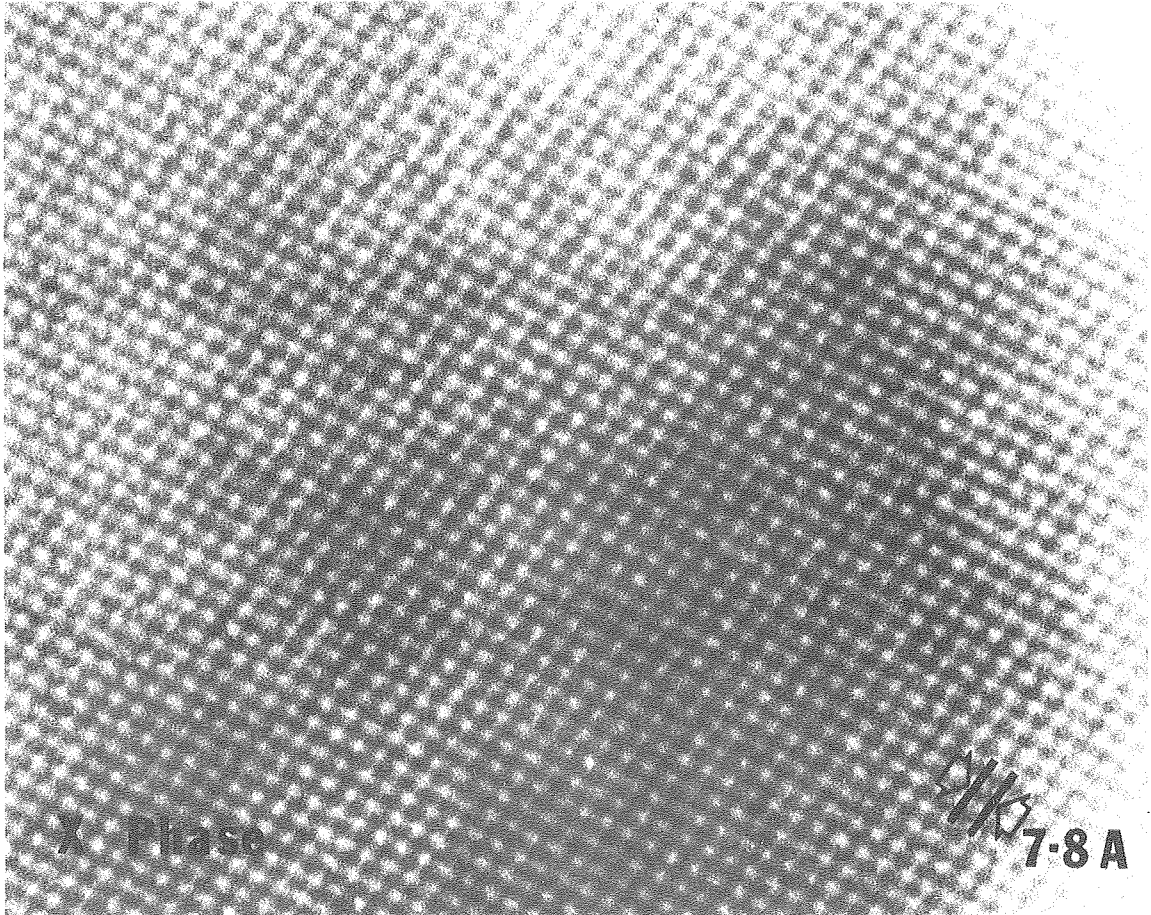
XBB 774-3250

FIG. 14

XBB 774-3248

FIG. 15